JACS
JOURNAL OF THE AMERICAN CHEMICAL SOCIETY
Article
Cite This: J. Am. Chem. Soc. XXXX, XXX, XXX−XXX
pubs.acs.org/JACS

Direct Asymmetric Ruthenium-Catalyzed Reductive Amination of Alkyl−Aryl Ketones with Ammonia and Hydrogen

Joan Gallardo-Donaire,[†,#] Marko Hermsen,[†,‡,#] Jedrzej Wysocki,[†] Martin Ernst,[§] Frank Rominger,[⊥] Oliver Trapp,[†,∥] A. Stephen K. Hashmi,[†,⊥] Ansgar Schäfer,[‡] Peter Comba,[†,▽] and Thomas Schaub*[,†,§]

[†]Catalysis Research Laboratory (CaRLa), Im Neuenheimer Feld 584, 69120 Heidelberg, Germany
[‡]BASF SE, Quantum Chemistry and Molecular Simulation, Carl-Bosch-Strasse 38, 67056 Ludwigshafen, Germany
[§]BASF SE, Synthesis and Homogeneous Catalysis, Carl-Bosch-Strasse 38, 67056 Ludwigshafen, Germany
[⊥]Organisch-Chemisches Institut, Heidelberg University, Im Neuenheimer Feld 270, 69120 Heidelberg, Germany
[∥]Department Chemie, Ludwig-Maximilians-Universität München, Butenandtstr. 5-13, 81377 München, Germany
[▽]Anorganisch-Chemisches Institut, Heidelberg University and Interdisciplinary Center for Scientific Computing (IWR), Im Neuenheimer Feld 270, 69120 Heidelberg, Germany

Supporting Information

ABSTRACT: The asymmetric ruthenium-catalyzed reductive amination employing ammonia and hydrogen to primary amines is described. Here we demonstrate the capability of our catalyst to perform a chemo- and enantioselective process while using simple ammonia gas as a reagent, one of the most attractive and industrially relevant nitrogen sources. The presence of a catalytic amount of ammonium iodide was essential for obtaining good yields and enantioselectivities. The mechanism of this reaction was investigated by DFT and we found a viable pathway that also explains the trend and magnitude of enantioselectivity through the halide series in good agreement with the experimental data. The in-depth investigation of substrate conformers during the reaction turned out to be crucial in obtaining an accurate prediction of the enantioselectivity. Furthermore, we report the crystallographic data of the chiral [Ru(I)H(CO)((*S*,*S*)-*f*-binaphane)(PPh_3)] complex, which we identified as the most efficient catalyst in our investigation.

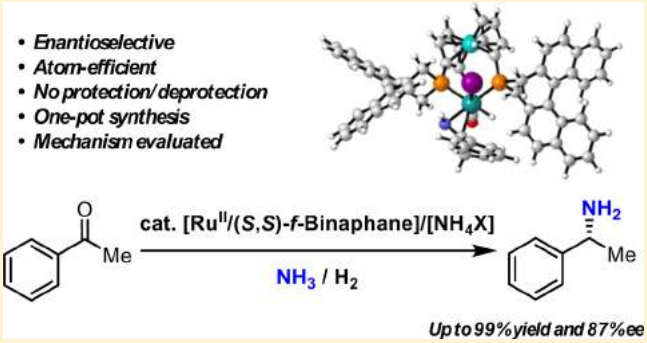

INTRODUCTION

Chiral amines are essential building blocks in organic synthesis and play an important role in pharmaceuticals and agrochemicals.[1] One of the most attractive approaches toward asymmetric amines relies on transition metal catalysis employing hydrogen as a reductant. In the last decades, enamine hydrogenation, imine hydrogenation, and reductive amination (RA)[2−10] have therefore become very popular due to the remarkable progress in catalyst and ligand design. RA represents *a priori* the most straightforward access to enantioenriched amines. However, most of the existing methodologies toward enantiomerically pure primary amines rely on multistep procedures consisting of *in situ* formation of a protected imine, followed by asymmetric hydrogenation and a final secondary amine deprotection step to generate the free primary amine (Scheme 1a).[11−18] In the last years, there was also much work involving biocatalytic approaches (mainly transamination using enzymes) to directly obtain enantiomerically pure primary amines from ketones.[19−24] Despite the remarkable progress and the many applications of the biocatalytic approach, a simple NH_3/H_2 could not be used as the reductive amination agent in these systems until today.

Another well-established protocol relies on transfer hydrogenation conditions mostly using stoichiometric amounts of ammonium formate (Leuckart−Wallach reaction) as both ammonia and hydrogen surrogate. Following this strategy, the first intermolecular enantioselective RA of ketones using a ruthenium catalyst with *tol*-BINAP as ligand was reported in 2003.[25] Despite achieving good enantioselectivities, the formylated amine is formed even under optimized conditions, thus requiring an extra hydrolysis step with concomitant generation of waste byproducts.

Despite the first asymmetric RA having been achieved in 1999 as the key step for the synthesis of (*S*)-metolachlor,[26] the scarcity of literature procedures for the direct reductive

Received: October 6, 2017
Published: December 1, 2017

DOI: 10.1021/jacs.7b10496
J. Am. Chem. Soc. XXXX, XXX, XXX−XXX

Scheme 1. State of the Art on Transition Metal Catalyzed Asymmetric Reductive Amination

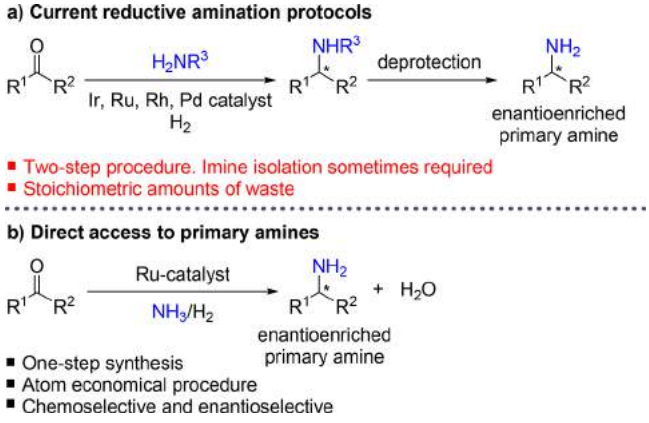

amination of ketones to primary amines using transition metal catalysts is surprising. The reasons for the slow progress in the field might be the following: (i) the carbonyl group used as starting material can be reduced by the catalyst to the corresponding alcohol, (ii) imine formation turns out to be slow unless water trapping agents were added, (iii) NH_3, intermediate imine, and the product can poison the catalyst, (iv) the generated imine intermediate potentially forms *E*/*Z* diastereoisomers, therefore making enantioinduction difficult, and (v) overalkylation to secondary and tertiary amines can occur. Therefore, no enantioselective RA with a simple NH_3/H_2 system has been reported to date. Taking into consideration our previous work on the reductive amination for the direct synthesis of primary amines with ammonia and hydrogen by means of ruthenium catalysis,[27−29] we were interested in developing the asymmetric variant as well, generating water as the only byproduct (Scheme 1b).

RESULTS AND DISCUSSION

Experimental Studies. Based on our nonasymmetric protocol, we performed an initial evaluation of our proposed concept with acetophenone (**1a**) as the model substrate, $[Ru(Cl)H(CO)(PPh_3)_3]$ as the ruthenium precursor, and $Al(OTf)_3$ as additive, using 6 bar of ammonia and 40 bar of hydrogen. In the optimization of the reaction conditions for the amination of the test substrate acetophenone, the use of toluene as solvent at 120 °C was identified as the best compromise between a sufficient substrate conversion and product selectivity.[30] A series of chiral ligands and additives were also systematically examined in the screening.

The most relevant results are summarized in Table 1. Considering the ability of dppe to efficiently promote this transformation, we tested Chiraphos (**L1**) as a potential chiral ligand (entry 1). Unfortunately, low conversion with low enantioselectivity was obtained. Other efficient ligands for asymmetric hydrogenation such as **L2**, **L3**, or **L4** provided very low stereoinduction (entries 2 and 4; for the results on the screening of 19 different chiral phosphines, see the Supporting Information). To our delight, (*S*,*S*)-*f*-binaphane[31−39] facilitates the desired coupling with excellent levels of chemoselectivity and enantiocontrol when employing 10 mol % of NH_4I as an additive (entry 9).

Having established the optimal conditions for our Ru-catalyzed RA, we examined the scope with respect to the ketone component. Currently, alkyl−aryl amines are by volume

Table 1. Ligand Screening[a]

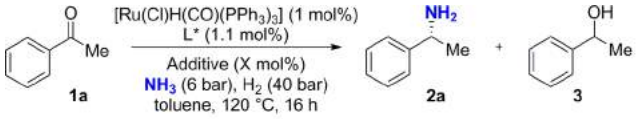

Entry	Ligand	Additive (X mol%)	2 (%)	3 (%)	*ee* (%)
1	L1	$Al(OTf)_3$ (10 mol%)	19	0	26
2	L2	$Al(OTf)_3$ (10 mol%)	2	10	n.d.
3	L3	$Al(OTf)_3$ (10 mol%)	65	12	21
4[b]	L4	$Al(OTf)_3$ (10 mol%)	26	6	23
5	L5	$Al(OTf)_3$ (10 mol%)	68	12	32
6	L6	$Al(OTf)_3$ (10 mol%)	80	0	13
7	L7	$NaPF_6$ (2 mol%)	67	9	70
8	L7	NH_4I (100 mol%)	68	12	32
g[c]	L7	NH_4I (10 mol%)	99	1	87
10	L7	–	10	33	–

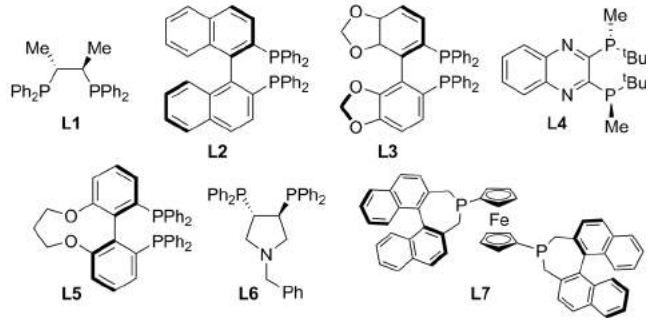

[a]Standard reaction conditions: 2.97 mmol of **1a**, Ru-catalyst (1 mol %), ligand (1.1 mol %), additive (*X* mol %), $p(NH_3)$ = 6 bar, $p(H_2)$ = 40 bar, toluene (20 mL), 120 °C, 16 h.. Yields determined by GC using dodecane as an internal standard. The *ee* values were determined by chiral HPLC after sample benzoylation. [b]Using Ru-precatalyst (2 mol %) and ligand (2.2 mol %). [c]Adding 2 mol % of $NaPF_6$. See the Supporting Information for the complete screening of additives and ligands.

the largest produced chiral amines by BASF using an enzymatic racemate resolution via selective acylation.[40] Therefore, we focused on the amination of acetophenone-like substrates. As revealed in Table 2, a wide range of substituted aromatic ketones could be efficiently aminated using NH_3/H_2 with moderate to high yields and enantioselectivity.

On one hand, 2-naphthyl methyl ketone **2b** provided 84% yield with 76% *ee*, but on the other hand, the reductive amination of 1-naphthyl methyl ketone failed, and the formation of **2s** was not observed. Taking the catalyst structure into account (see below), it seems feasible that the corresponding imine is not able to coordinate to the ruthenium due to steric hindrance of the 1-naphthyl group. Both electron-donating and electron-withdrawing groups are tolerated (**2c** and **2d**) to a certain extent providing 82% *ee* and 79% *ee*, respectively. But in case of a *para*-fluoro substituent, the yield drops to 34%. With the stronger electron withdrawing *para*-CF_3 group, the desired amine **2t** is formed in an even lower yield of 20% and an *ee* of only 42%. In contrast, CF_3 groups in the *meta* positions are compatible as shown in the formation of **2h**. Interestingly, aryl chlorides are compatible with our reductive amination protocol as shown by **2f** and **2i**, therefore leaving further opportunities for a subsequent cross-coupling derivatization. The thiomethyl group provided a good level of

DOI: 10.1021/jacs.7b10496
J. Am. Chem. Soc. XXXX, XXX, XXX−XXX

Table 2. Substrate Scope

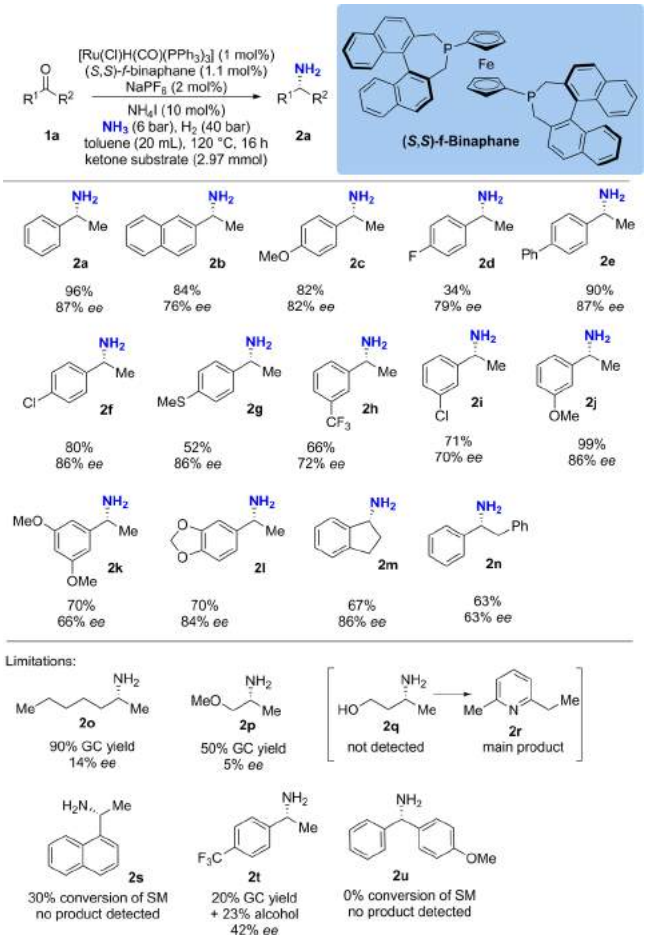

Chart 1. Halide Effect on the Reaction Outcome

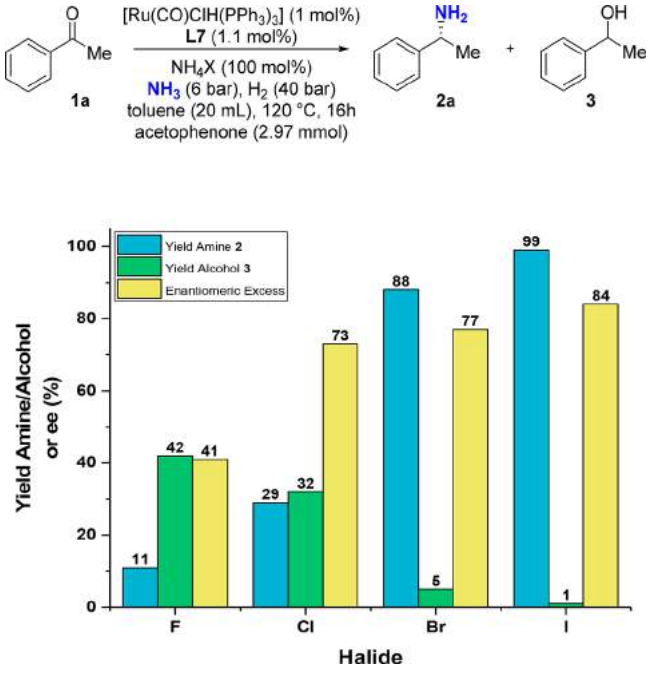

enantioinduction, albeit in a lower yield (**2g**). Despite being optimized for the amination of α-methyl-aryl-ketones, the protocol also works for related substrates as exemplified by **2m**, providing 67% yield and 86% *ee* and **2n** with a comparable yield 63% but only a modest *ee* of 64%.

In contrast to the acetophenone-like substrates, the protocol does not work with simple alkyl or diaryl ketones. For example, when 2-heptanone is used as the substrate, the chemoselectivity is still good as **2o** is formed in about 90% yield, but the *ee* is negligible (14%). In case of 1-methoxy-2-propanone, the amine is formed in 50% yield, although hardly any *ee* was observed. For the amination of alkyl ketones, the system must be further modified in order to achieve acceptable enantioselectivity. When 4-hydroxy-2-butanone is used, the picture changes completely: Not the desired amine **2q** is formed; instead pyridine **2r** is the main product.[41] Interestingly, the diaryl ketone 4-methoxy-benzophenone is not touched at all using this protocol, and the starting material was recovered.[42]

We were intrigued by the role of the additive considering its remarkable impact on both chemo- and stereoselectivity. Halides as ancillary ligands have been shown to be efficient when fine-tuning the reactivity of transition metal-catalyzed processes.[43] The results presented in Chart 1 summarize the halide effect on the reaction outcome.

The selectivity of primary amine versus alcohol (reduced starting material) increases when increasing the σ-donation to the metal center, obtaining the best ratios with bromide and iodide. Moreover, the enantioselectivity was also improved when increasing the steric bulk on the halide, probably due to a halide exchange on the ruthenium center. During efforts to gain more insights into the origins of chemo- and enantioselectivity, we reacted the precursor $[Ru(Cl)H(CO)(PPh_3)_3]$ with (*S,S*)-*f*-binaphane in the presence of NH_4I and NH_3/H_2 pressure and were able to identify the ruthenium complex $[Ru(I)H(CO)((S,S)$-*f*-binaphane$)(PPh_3)]$ (**4**) as the main species (see Supporting Information for more details). The composition of **4** could be determined by NMR, IR, mass spectrometry (MS), and X-ray diffraction. In the proton NMR spectrum, the hydrido ligand appears as a doublet of doublets of doublets at −7.86 ppm due to the coupling with three different phosphorus atoms. In the $^{31}P\{^1H\}$ NMR, the signals for the coordinated binaphane are detected as doublet of doublets at 53.8 and 34.8 ppm, and that for the remaining PPh_3 ligand is detected as an overlapped signal of two doublets at 25.9 ppm. In the IR spectrum, the signal for the carbonyl ligand is observed as a strong signal at 1935 cm^{-1}, and in the FD-MS the molecular peak for **4** is found at 1326.1005 (calculated for $C_{72}H_{56}FeIOP_3Ru$ = 1326.0982), confirming the exchange of the chloride ligand of the precursor to an iodo ligand. Despite many attempts, we were not able to prepare **4** in the bulk in analytically pure form, as complete removal of free PPh_3 formed during the reaction with $[Ru(Cl)H(CO)(PPh_3)_3]$ was not possible and also some other minor Ru species were formed. By diffusion of *n*-pentane into a solution of **4** in CH_2Cl_2 we were at least able to obtain crystals suitable for X-ray diffraction, which confirmed the composition and structure of **4** (Figure 1). As expected, the carbonyl is located *trans* to the iodide. The hydride ligand at the Ru center could not be localized in the difference electron density map. However, the charge balance, the geometry of the complex, and the *trans* distance Ru−P2 of 2.43 Å clearly indicate its presence. Despite not being a proof, the structure suggests a halide exchange on the metal center, thus creating a more sterically encumbered chiral pocket, which accounts for the higher enantioselectivity observed in the presence of an iodide source such as ammonium iodide.

DOI: 10.1021/jacs.7b10496
J. Am. Chem. Soc. XXXX, XXX, XXX−XXX

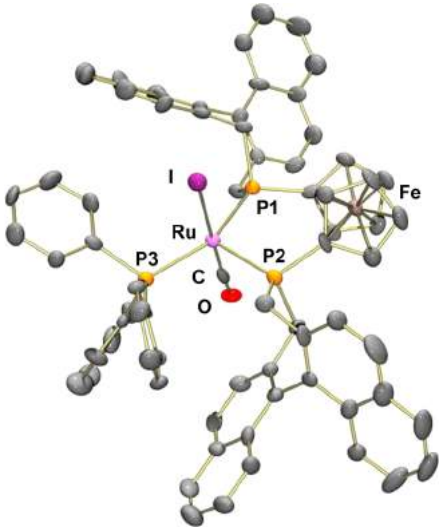

Figure 1. Molecular structure of [Ru(I)H(CO)((*S*,*S*)-*f*-binaphane)-(PPh_3)] (**4**) complex.[44] Thermal ellipsoids are at 50% probability. Hydrogen atoms are omitted for clarity. Selected bond lengths [Å] and angles [deg]: Ru−I 2.7932(9), Ru−C 1.834(10), Ru−P1 2.340(2), Ru−P2 2.434(3), Ru−P3 2.404(2), C−O 1.138(9), I−Ru−C 179.0(3), P3−Ru−I 84.59(5), P3−Ru−P1 155.63(2), P2−Ru−C 90.5(3), Ru−C−O 175.6(7).

Computational Study. To shed light on the mechanism of the reaction and to explain the observed enantio- and chemoselectivity, we conducted detailed computational studies. All geometries were optimized at the BP86/def2-SV(P) level[45−47] with effective core potentials for ruthenium. Final electronic energies were obtained at the PBE0-D3(BJ)/def2-QZVPP level[48] with dispersion correction using Becke−Johnson damping.[49,50] All electronic structure calculations were carried out with the TURBOMOLE program[51] using the resolution-of-identity approximation[52] and the corresponding auxiliary basis sets.[53,54] Zero-point vibrational energies and thermodynamic corrections were calculated at the level of geometry optimization with T = 298.15 K and p = 1 bar. For all species, the thermodynamic reference was χ = 0.01, except for hydrogen (p = 40 bar) and ammonia (p = 6 bar). Solvent corrections to free enthalpies were calculated for toluene with the conductor-like screening model for real solvents[55] (COSMO-RS) carried out with COSMOtherm[56] (version C3.0, release 1501, revision 1744). The single-ended growing string method[57,58] was employed in the search for some of the transition states. All energies discussed are free enthalpies (G) in kJ/mol with solvent correction.

Challenges. We first set out to identify the most likely catalytic species. Experimental observations suggested that besides the binaphane ligand and hydride, CO, and halide ion are coordinated to the ruthenium to facilitate the reaction, leaving one free coordination site for the imine substrate. All the different possible isomers were initially studied for the binaphane hydride iodide complex where we substituted the free site with ammonia. Of six combinatorially possible isomers, only the two isomer types **A** and **B** seemed energetically viable (see Supporting Information), both of which have the hydride and active site (coordinating either substrate or PPh_3) *trans* to the binaphane ligand while halide and CO occupy the apical positions as can be seen in Figure 2.

Interchanging either halide and CO or hydride and the substrate site converts one isomer into the other, due to the C_2 symmetry of the ligand. The crystal structure of isomer **B** (see Figure 1), confirms the computational expectation.

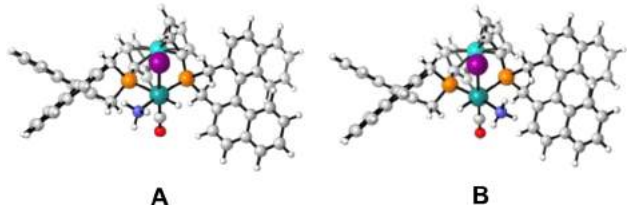

Figure 2. Structures of isomer types **A** and **B**. In catalysis, the coordination site of ammonia is where the substrate would bind. Other isomer types where the CO ligand is *trans* to the binaphane ligand were too high in energy to be viable (see Supporting Information).

In our proposed catalytic cycle (see Scheme 2), the substrate coordinates to the active site, subsequently forming the η^2 complex, which can then undergo the enantioselectivity-determining hydride transfer to the substrate resulting in the trigonal planar amide. Hydrogen then coordinates to form the corresponding σ-complex. The coordinated hydrogen will transfer a proton to the amide nitrogen, which is the rate-determining step, finally liberating the chiral amine and restoring the initial hydride complex through heterolytic cleavage of the H−H bond.

Scheme 2. Proposed Mechanism for the Asymmetric Imine Hydrogenation

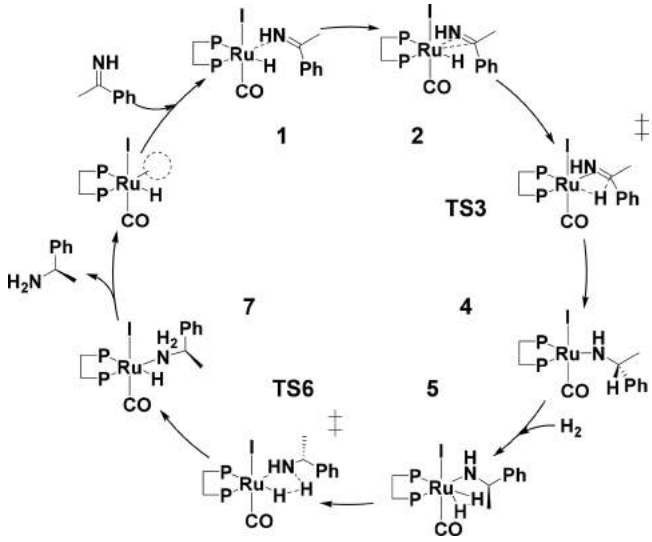

The main challenge in investigating such a mechanism is the number of (conformational) isomers that have to be examined. While other mechanistic investigations do not necessarily fail when not all conformers are considered, the subtle energetic effects that drive enantioselectivity and the structural and steric interactions in this case demand a thorough treatment of all possible isomers that may play a role in the course of the reaction.

For the η^2-imine complex, the hydride transfer transition state (**TS6**), and the agostic amide complex, both complex isomers **A** and **B**, *E* and *Z* configuration of the imine, and both *R* and *S* face of the imine coordinating to ruthenium have to be taken into account, resulting in eight potential isomers. Upon hydrogen addition to the complex, the σ-dihydrogen/amide complex and proton transfer transition state can similarly have

DOI: 10.1021/jacs.7b10496
J. Am. Chem. Soc. XXXX, XXX, XXX−XXX

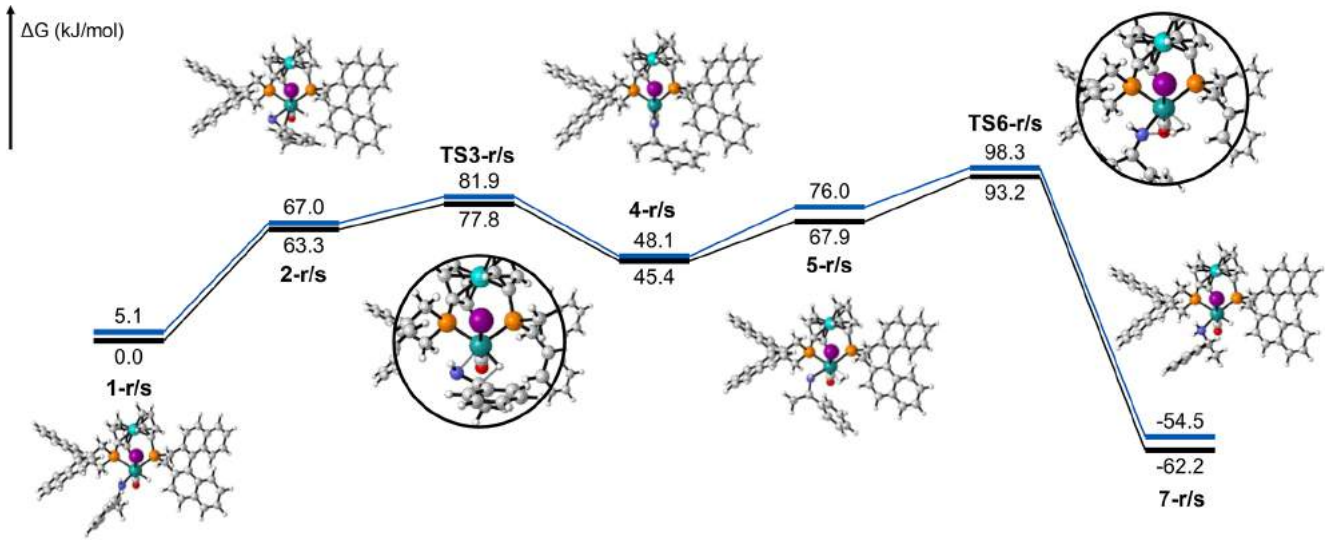

Figure 3. Lowest energy paths in the catalytic cycle leading to the *R* (black) and *S* (blue) enantiomer of 1-phenylethylamine. Formation of the *R* enantiomer occurs mainly through a complex of type **A**, while the *S* enantiomer is mainly formed by a complex of type **B**. For clarity, structures are only shown for the *R* pathway. For the proton transfer (**TS3-r**) and hydride transfer (**TS6-r**) transition states, the center of reaction has been magnified.

potentially 24 different isomers and conformers, as will be shown later (see also the Supporting Information for more details).

Mechanism. The lowest energetic pathway to both the *R* and *S* enantiomer of acetophenone are shown in Figure 3. Note that two different general isomers are involved: while the complex of isomer type **A** leads to formation of the *R* enantiomer, type **B** leads to the formation of the *S* enantiomer. Starting from complex **1-r/s**, where the imine is coordinated to the ruthenium catalyst, the imine then forms the η^2-complex **2-r/s** with π-coordination of the imine double bond to the ruthenium metal center. This step is endergonic by 63.3 kJ/mol (*R*) and 67.0 kJ/mol (*S*). The following hydride transfer transition states **TS3-r/s** are only slightly higher in energy with 81.9 kJ/mol (*R*) and 77.8 kJ/mol (*S*) relative to **1-r**. Interestingly, the corresponding hydride transfers of *R*-**B** and *S*-**A** are lower in energy (70.2 kJ/mol for *R*, 71.5 kJ/mol for *S*). However, since the rate-determining step is the proton transfer, they lead to the "wrong" or energetically unfavorable intermediates for the later transition state **TS6**. As mentioned above, eight possible hydride transfers pathways exist. The lowest two have the imine hydrogen pointing toward the iodide with a hydrogen-bond-like stabilization; they also avoid the unfavorable anion−π interaction by having the phenyl group facing the carbonyl ligand instead of the halide and require the imine to be in *E* configuration, which is favored by 3.1 kJ/mol (for the uncoordinated imine). **TS3-r/s** also have a hydrogen-bond-like interaction but are *Z* configurated with the phenyl group toward the halide, emerging in a repulsive anion−π interaction. The remaining four hydride transfer transition states are all higher in energy as they lack the NH−I interaction of the other four (see Supporting Information). Following hydride transfer, the trigonal planar complexes **4-r/s** are formed (45.4 kJ/mol for *R* and 48.1 kJ/mol for *S*). Addition of hydrogen to **4r/s** forms the σ-dihydrogen/amide complexes **5-r/s**, which are destabilized by 22.5 kJ/mol (*R*) and 27.9 kJ/mol (*S*) with respect to **4-r/s**. The σ-dihydrogen then undergoes heterolytic H−H bond cleavage through protonation of the amide, forming the final amine and ruthenium hydride complex **7-r/s** via proton transfer transition state **TS6-r/s**. The proton transfer is the rate-determining step in the catalytic cycle with an overall barrier of 93.2 kJ/mol for the *R* enantiomer and 98.3 kJ/mol for the *S* enantiomer. In accordance with experimental results, it predicts a preference of *R* over *S*. Since the C−N single bond can rotate freely, many (conformational) isomers may possibly be responsible for this step. A first examination showed that only considering some of these would yield almost random results, which made a thorough analysis of all conformers inevitable. Exploring the different amide conformers, we sorted them by four geometric properties: complex type **A** or **B**, amide hydrogen pointing toward halide or CO, *R* or *S* amide, and last hydrogen, phenyl, or methyl group being anti to the amide hydrogen, giving potentially 2 × 2 × 2 × 3 = 24 conformers. Not all of these can be found as some would require impossible orientations of the amide (e.g., phenyl group pointing into the binaphthyl moiety of the ligand), but a careful examination of all of them is still required for a precise understanding of the origin of the stereoselectivity. The energetically lowest barriers, **TS6-r/s**, are shown in Figure 3. Similar to the hydride transfer transition states, we find that the amide hydrogen/halide interaction generally stabilizes transition states. The lowest energy transition states minimize steric repulsion between the phenyl/methyl group of the amide and the binaphthyl groups of the ligand or have attractive π−π interactions, see Supporting Information for details. Finally, the formation of amine/hydride complex **7-r/s** is strongly exergonic by 155.4 kJ/mol (*R*) and 152.8 kJ/mol (*S*). This means that this last step is irreversible and complexes **7-r/s** regenerate the initial complex **1-r/s** by release of the amine and coordination of imine. Exchange of the amine for an imine is thermodynamically slightly favored (3.3 kJ/mol for **7r** to **1r** and 5.8 kJ/mol for **7s** to **1s**).

Halide Effect on Enantioselectivity. The choice of halide has a strong influence on the enantioselectivity as shown in Figure 4. We recalculated the catalytic pathway for the other three halides using the most stable η^1-imine complex as reference in each case. The proton transfer remains the rate-determining step and therefore controls stereoselectivity. Based

DOI: 10.1021/jacs.7b10496
J. Am. Chem. Soc. XXXX, XXX, XXX−XXX

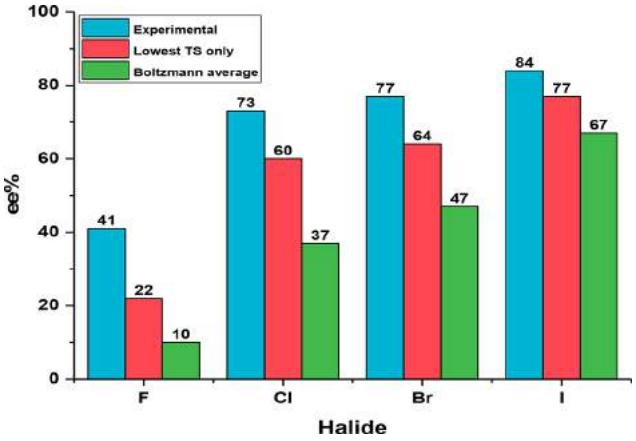

Figure 4. Comparison of experimentally observed and calculated enantiomeric excess for the reductive amination of acetophenone with the Ru-*S*,*S*-*f*-binaphane system using different halides.

on the barrier difference, $\Delta\Delta G^{\ddagger}$, we estimated the enantiomeric excess that is expected according to our mechanism.

As depicted in Figure 4, the calculated enantiomeric excess is in very good agreement with our experimental results, reproducing both trend and magnitude of the observed enantioselectivity. We made two estimates: one based only on the lowest two transition states leading to the *R* and *S* enantiomer and a second that Boltzmann-averages over all found proton transfer transition states (slightly higher deviation). Both are in good agreement with our experimental results, especially when considering the exponential relationship between $\Delta\Delta G^{\ddagger}$ and *ee* and the small energy differences involved (only ∼5.7 kJ/mol separate 0% and 90% *ee*).

Chemoselectivity. The different halides also influence the chemoselectivity (see Chart 1). Especially the difference between iodide, where almost only hydrogenation of the imine is observed, and fluoride, which prefers hydrogenation of the ketone over the imine, is striking. We therefore investigated the corresponding hydrogenation of the ketone in both cases. Our proposed mechanism confirms that imine hydrogenation should be preferred by the iodide catalyst by 32.6 kJ/mol but similarly predicts that the fluoride catalyst should also be chemoselective toward the amine by 23.7 kJ/mol. A different mechanism is therefore likely to be responsible for the formation of alcohol in the case of the fluoride catalyst. We propose an alternative pathway in which catalytic amounts of HF are responsible for protonation of the alkoxide. HF is far more likely to be present than HI in an analogous mechanism for the iodide catalyst, as the dissociation constants of HF and HI differ by ∼13 orders of magnitude.[59] Furthermore, an excess of NH_4F is used, which is also known to dissociate into ammonia and HF upon heating.[60]

As HF does not form the corresponding σ-complex like dihydrogen, a direct addition to the trigonal amide/alkoxide complex is most likely, resulting in a difluoride-amine/alcohol complex. In search for the corresponding transition state for this step, we found that, due to the reactivity of HF, this process seems to occur barrierlessly. This explains the loss of chemoselectivity, as in the presence of HF, the proton transfer from H_2, which was responsible for the chemoselectivity, is no longer necessary to release either amine or alcohol. Upon release of the product and coordination of H_2 to the active site, regeneration of the initial hydride complex occurs very rapidly from the dihydrogen/difluoride complex as the activation energy for this step is only 36.8 or 40.1 kJ/mol (isomer types **A**/**B**).

CONCLUSION

The direct asymmetric amination of alkyl−aryl ketones with ammonia and hydrogen to primary amines with good enantio- and chemoselectivity has been achieved for a series of substrates, using a ruthenium (*S*,*S*)-*f*-binaphane catalyst with iodide as an additive. The addition of iodide to the catalyst system is essential for the selectivity. An X-ray structure of the catalyst **4** was obtained, showing the coordination of iodide to the ruthenium complex. Computational investigations show that the proposed mechanism is energetically feasible and can accurately reproduce the experimentally observed enantioselectivity. This is only possible through a thorough investigation of all possible conformers in the rate-determining protonation step. As for the chemoselectivity, our calculations indicate that the change toward ketone hydrogenation with fluoride as an additive is promoted by HF, a pathway not accessible for iodide. Our method provides an atom-efficient access to a large class of industrially relevant chiral amines, employing only ammonia and hydrogen without the need for derivatization or deprotection and therefore avoiding multistep procedures. The protocol is not directly adaptable for the asymmetric amination of dialkyl or diaryl ketones. Therefore, we want to use the gained mechanistic insights to further modify the catalyst in order to apply the asymmetric reductive amination with NH_3/H_2 to dialkyl or diaryl ketones for the synthesis of the corresponding enantiomeric pure amines. But as diaryl amines are not reacting under the conditions of the presented system, this behavior can also be useful. For example, it could allow the application of this system to multifunctional substrates for the selective amination of an aryl−alkyl ketone group in the presence of a diaryl substituted ketone function.

ASSOCIATED CONTENT

Supporting Information

The Supporting Information is available free of charge on the ACS Publications website at DOI: 10.1021/jacs.7b10496.

Crystallographic data of isolated complex (CIF)
Detailed experimental procedures and analyses, NMR spectra, HPLC chromatograms and computational details (PDF)

AUTHOR INFORMATION

Corresponding Author

*thomas.schaub@basf.com

ORCID

Oliver Trapp: 0000-0002-3594-5181
A. Stephen K. Hashmi: 0000-0002-6720-8602
Peter Comba: 0000-0001-7796-3532
Thomas Schaub: 0000-0003-2332-0376

Author Contributions

#J.G.-D. and M.H. contributed equally.

Notes

The authors declare no competing financial interest.

ACKNOWLEDGMENTS

CaRLa (Catalysis Research Laboratory) is cofinanced by the Ruprecht-Karls-Universität Heidelberg (Heidelberg University) and BASF SE.

DOI: 10.1021/jacs.7b10496
J. Am. Chem. Soc. XXXX, XXX, XXX−XXX

REFERENCES

(1) Breuer, M.; Ditrich, K.; Habicher, T.; Hauer, B.; Kesseler, M.; Sturmer, R.; Zelinski, T. *Angew. Chem., Int. Ed.* **2004**, *43*, 788−824.
(2) Gomez, S.; Peters, J. A.; Maschmeyer, T. *Adv. Synth. Catal.* **2002**, *344*, 1037−1057.
(3) Nugent, T. C.; El-Shazly, M. *Adv. Synth. Catal.* **2010**, *352*, 753−819.
(4) Xie, J. H.; Zhu, S. F.; Zhou, Q. L. *Chem. Rev.* **2011**, *111*, 1713−1760.
(5) Tang, W.; Xiao, J. *Synthesis* **2014**, *46*, 1297−1302.
(6) Wang, C.; Xiao, J. *Top. Curr. Chem.* **2013**, *343*, 261−282.
(7) Xie, J. H.; Zhu, S. F.; Zhou, Q. L. *Chem. Soc. Rev.* **2012**, *41*, 4126−4139.
(8) Huang, H.; Liu, X.; Zhou, L.; Chang, M.; Zhang, X. *Angew. Chem., Int. Ed.* **2016**, *55*, 5309−5312.
(9) Steinhuebel, D.; Sun, Y.; Matsumura, K.; Sayo, N.; Saito, T. *J. Am. Chem. Soc.* **2009**, *131*, 11316−11317.
(10) Huang, H.; Zhao, Y.; Yang, Y.; Zhou, L.; Chang, M. *Org. Lett.* **2017**, *19*, 1942−1945.
(11) Tararov, V. I.; Kadyrov, R.; Börner, A.; Riermeier, T. H. *Chem. Commun.* **2000**, 1867−1868.
(12) Li, C.; Wang, C.; Villa-Marcos, B.; Xiao, J. *J. Am. Chem. Soc.* **2008**, *130*, 14450−14451.
(13) Rubio-Perez, L.; Perez-Flores, F. J.; Sharma, P.; Velasco, L.; Cabrera, A. *Org. Lett.* **2009**, *11*, 265−268.
(14) Chang, M.; Liu, S.; Huang, K.; Zhang, X. *Org. Lett.* **2013**, *15*, 4354−4357.
(15) Zhang, Y.; Lim, C. S.; Sim, D. S.; Pan, H. J.; Zhao, Y. *Angew. Chem., Int. Ed.* **2014**, *53*, 1399−1403.
(16) Hou, G.; Gosselin, F.; Li, W.; McWilliams, J. C.; Sun, Y.; Weisel, M.; O'Shea, P. D.; Chen, C. Y.; Davies, I. W.; Zhang, X. *J. Am. Chem. Soc.* **2009**, *131*, 9882−9883.
(17) Hou, G.; Tao, R.; Sun, Y.; Zhang, X.; Gosselin, F. *J. Am. Chem. Soc.* **2010**, *132*, 2124−2125.
(18) Zhao, Q.; Wen, J.; Tan, R.; Huang, K.; Metola, P.; Wang, R.; Anslyn, E. V.; Zhang, X. *Angew. Chem., Int. Ed.* **2014**, *53*, 8467−8470.
(19) Fuchs, M.; Farnberger, J. E.; Kroutil, W. *Eur. J. Org. Chem.* **2015**, *2015*, 6965−6982.
(20) Burns, M.; Martinez, C. A.; Vanderplas, B.; Wisdom, R.; Yu, S.; Singer, R. A. *Org. Process Res. Dev.* **2017**, *21*, 871−877.
(21) Guo, F.; Berglund, P. *Green Chem.* **2017**, *19*, 333−360.
(22) Liardo, E.; Ríos-Lombardía, N.; Morís, F.; Rebolledo, F.; González-Sabín, J. *ACS Catal.* **2017**, *7*, 4768−4774.
(23) Holzer, A. K.; Hiebler, K.; Mutti, F. G.; Simon, R. C.; Lauterbach, L.; Lenz, O.; Kroutil, W. *Org. Lett.* **2015**, *17*, 2431−2433.
(24) Sun, H.; Zhang, H.; Ang, E. L.; Zhao, H. *Bioorg. Med. Chem.* **2017**, DOI: 10.1016/j.bmc.2017.06.043.
(25) Kadyrov, R.; Riermeier, T. H. *Angew. Chem., Int. Ed.* **2003**, *42*, 5472−5474.
(26) Blaser, H.-U.; Buser, H.-P.; Jalett, H.-P.; Pugin, B.; Spindler, F. *Synlett* **1999**, *1999*, 867−868.
(27) Ye, X.; Plessow, P. N.; Brinks, M. K.; Schelwies, M.; Schaub, T.; Rominger, F.; Paciello, R.; Limbach, M.; Hofmann, P. *J. Am. Chem. Soc.* **2014**, *136*, 5923−5929.
(28) Derrah, E. J.; Hanauer, M.; Plessow, P. N.; Schelwies, M.; da Silva, M. K.; Schaub, T. *Organometallics* **2015**, *34*, 1872−1881.
(29) Gallardo-Donaire, J.; Ernst, M.; Trapp, O.; Schaub, T. *Adv. Synth. Catal.* **2016**, *358*, 358−363.
(30) The influence of ligands, solvents, additives, and temperature was investigated in a screening using acetophenone as test substrate to identify optimal conditions for a high substrate conversion and good selectivities; the results for the whole screening are given in the Supporting Information.
(31) Xiao, D.; Zhang, Z.; Zhang, X. *Org. Lett.* **1999**, *1*, 1679−1681.
(32) Xiao, D.; Zhang, X. *Angew. Chem.* **2001**, *113*, 3533−3536.
(33) Chi, Y.; Zhou, Y. G.; Zhang, X. *J. Org. Chem.* **2003**, *68*, 4120−4122.
(34) Tang, W.; Wang, W.; Chi, Y.; Zhang, X. *Angew. Chem., Int. Ed.* **2003**, *42*, 3509−3511.
(35) Corkey, B. K.; Toste, F. D. *J. Am. Chem. Soc.* **2007**, *129*, 2764−2765.
(36) Wang, Y. Q.; Yu, C. B.; Wang, D. W.; Wang, X. B.; Zhou, Y. G. *Org. Lett.* **2008**, *10*, 2071−2074.
(37) Li, W.; Hou, G. H.; Chang, M. X.; Zhang, X. M. *Adv. Synth. Catal.* **2009**, *351*, 3123−3127.
(38) Hou, G.; Li, W.; Ma, M.; Zhang, X.; Zhang, X. *J. Am. Chem. Soc.* **2010**, *132*, 12844−12846.
(39) Chang, M.; Li, W.; Zhang, X. *Angew. Chem., Int. Ed.* **2011**, *50*, 10679−10681.
(40) Karl, U.; Simon, A. *chimica oggi − Chemistry Today* **2009**, *27*, 66−69.
(41) The cyclization of *β*-amino alcohols with alcohols to substituted pyridines using ruthenium and iridium catalysts was reported previously. Probably the unreacted starting material reacts in this case with the *in situ* formed amine, followed by further condensation/hydrogenations to give the corresponding pyridine **2r**. See (a) Michlik, S.; Kempe, R. *Angew. Chem., Int. Ed.* **2013**, *52*, 6326−6329. (b) Srimani, D.; Ben-David, Y.; Milstein, D. *Chem. Commun.* **2013**, *49*, 6632−6634.
(42) Despite that imines derived from benzophenones and ammonia are relatively stable, the imine of *p*-methoxybenzophenone was not detected after the reaction. Formation of this imine from NH_3 usually requires much higher NH_3 pressures (50−60 bar) and the addition of stoichiometric amounts of NH_4Cl. See: Verardo, G.; Giumanini, A. G.; Strazzolini, P.; Poiana, M. *Synth. Commun.* **1988**, *18*, 1501−1511.
(43) Fagnou, K.; Lautens, M. *Angew. Chem., Int. Ed.* **2002**, *41*, 26−47.
(44) The hydride ligand at the Ru center could not be localized in the difference electron density map. However, the charge balance, the geometry of the complex, and the trans distance Ru1−P3 of 2.43 Å indicate clearly its presence.
(45) Perdew, J. P. *Phys. Rev. B: Condens. Matter Mater. Phys.* **1986**, *33*, 8822−8824.
(46) Becke, A. D. *Phys. Rev. A: At., Mol., Opt. Phys.* **1988**, *38*, 3098−3100.
(47) Weigend, F.; Ahlrichs, R. *Phys. Chem. Chem. Phys.* **2005**, *7*, 3297−305.
(48) Ernzerhof, M.; Scuseria, G. E. *J. Chem. Phys.* **1999**, *110*, 5029−5036.
(49) Grimme, S.; Antony, J.; Ehrlich, S.; Krieg, H. *J. Chem. Phys.* **2010**, *132*, 154104.
(50) Grimme, S.; Ehrlich, S.; Goerigk, L. *J. Comput. Chem.* **2011**, *32*, 1456−1465.
(51) TURBOMOLE V7.0; TURBOMOLE GmbH: Karlsruhe, Germany, 2015. http://www.turbomole.com.
(52) Weigend, F. *Phys. Chem. Chem. Phys.* **2006**, *8*, 1057−1065.
(53) Weigend, F.; Häser, M.; Patzelt, H.; Ahlrichs, R. *Chem. Phys. Lett.* **1998**, *294*, 143−152.
(54) Hellweg, A.; Hattig, C.; Hofener, S.; Klopper, W. *Theor. Chem. Acc.* **2007**, *117*, 587−597.
(55) Eckert, F.; Klamt, A. *AIChE J.* **2002**, *48*, 369−385.
(56) COSMOtherm, Version C3.0, Release 1501; COSMOlogic GmbH & Co KG: Leverkusen, Germany, 2014. http://www.cosmologic.de.
(57) Zimmerman, P. M. *J. Comput. Chem.* **2015**, *36*, 601−611.
(58) molecularGSM repository on Github. https://github.com/ZimmermanGroup/molecularGSM (accessed August 8, 2017).
(59) Cotton, F. A.; Wilkinson, G.; Murillo, C. A.; Bochmann, M. *Advanced Inorganic Chemistry*, 6th ed.; Wiley: New York, 1999.
(60) Aigueperse, J.; Mollard, P.; Devilliers, D.; Chemla, M.; Faron, R.; Romano, R.; Cuer, J. P. Fluorine Compounds, Inorganic. *Ullmann's Encyclopedia of Industrial Chemistry*; Wiley, 2000.

DOI: 10.1021/jacs.7b10496
J. Am. Chem. Soc. XXXX, XXX, XXX−XXX